

# 1 Evident PM<sub>2.5</sub> Drops in the East of China due to the COVID-19 2 Quarantines in February

3 Zhicong Yin<sup>123</sup>, Yijia Zhang<sup>1</sup>, Huijun Wang<sup>123</sup>, Yuyan Li<sup>1</sup>

4 <sup>1</sup>Key Laboratory of Meteorological Disaster, Ministry of Education / Joint International Research Laboratory of Climate and  
5 Environment Change (ILCEC) / Collaborative Innovation Center on Forecast and Evaluation of Meteorological Disasters  
6 (CIC-FEMD), Nanjing University of Information Science & Technology, Nanjing, 210044, China

7 <sup>2</sup>Southern Marine Science and Engineering Guangdong Laboratory (Zhuhai), Zhuhai, 519080, China

8 <sup>3</sup>Nansen-Zhu International Research Centre, Institute of Atmospheric Physics, Chinese Academy of Sciences, Beijing, China

9 *Correspondence to:* Zhicong Yin (yinzhc@163.com)

10 **Abstract.** The top-level emergency response to the COVID-19 pandemic involved an exhaustive quarantine in China. The  
11 impacts of COVID-19 quarantine on the decline in fine particulate matter (PM<sub>2.5</sub>) were quantitatively assessed based on  
12 numerical simulations and observations in February. Relative to both of February 2017 and climate mean, anomalous  
13 southerlies and moister air occurred in the east of China in February 2020, which caused considerable PM<sub>2.5</sub> anomalies. Thus,  
14 it is a must to disentangle the contributions of stable meteorology from the effects of the COVID-19 lockdown. The  
15 contributions of routine emission reductions were also quantitatively extrapolated. The top-level emergency response  
16 substantially alleviated the level of haze pollution in the east of China. Although climate variability elevated the PM<sub>2.5</sub> by 29%  
17 (relative to 2020 observations), 59% decline related to COVID-19 pandemic and 20% decline from the expected pollution  
18 regulation dramatically exceeded the former in North China. The COVID-19 quarantine measures decreased the PM<sub>2.5</sub> in  
19 Yangtze River Delta by 72%. In Hubei Province where most pneumonia cases were confirmed, the impact of total emission  
20 reduction (72%) evidently exceeded the rising percentage of PM<sub>2.5</sub> driven by meteorology (13%).

21 **Keywords:** COVID-19, PM<sub>2.5</sub>, Emission Reduction, Climate Variability, Haze

## 22 1 Introduction

23 The COVID-19 pandemic devastatingly swept through China in the beginning of 2020 (Luo, 2020; Xia et al., 2020; Cao  
24 et al., 2020). By April 2020, more than 84 thousand confirmed cases were reported by the National Health Commission of  
25 China, approximately 75% of which were confirmed in February (Fig. 1a). To effectively control the large spread of COVID-  
26 19 pneumonia, stringent quarantine measures were implemented by the Chinese government and people themselves, including  
27 prohibiting social activities, shuttering industries, stopping transportation, etc. (Chen S. et al., 2020). The abovementioned  
28 emergency response measures were first carried out in Wuhan on 23 January, which resulted in the delayed arrival of COVID-  
29 19 in other cities by 2.91 days, and these response measures were in effect in all cities across China, thus limiting the spread  
30 of the COVID-19 epidemic in China (Tian et al., 2020). Since March 7, the number of newly confirmed cases in China has

31 been nearly below 100. On the other hand, the COVID-19 quarantine measures greatly reduced anthropogenic emissions, and  
32 therefore, the air quality in China was considerably improved (Wang et al., 2020). Chen K. et al. (2020) simply compared  
33 observations of atmospheric components before and during the quarantine and found that the concentration of fine particulate  
34 matter (PM<sub>2.5</sub>) in Wuhan decreased 1.4  $\mu\text{g}/\text{m}^3$ , but it decreased 18.9  $\mu\text{g}/\text{m}^3$  in 367 cities across China. Shi et al. (2020) quantified  
35 a 35% reduction of PM<sub>2.5</sub> on average during the COVID-19 outbreak compared to the pre-COVID-19 period. Huang et al.  
36 (2020) used comprehensive measurements and modeling to show that the haze during COVID-19 lockdown was driven by  
37 enhancements of secondary pollution, which offset reduction of primary emissions during this period in China. However, the  
38 impacts of meteorology on the air quality were neglected in many previous studies.

39 Climate variability notably influences the formation and intensity of haze pollution in China (Yin and Wang 2016; Xiao  
40 et al., 2015; Zou et al., 2017), and the impacts are embodied by variations in surface wind, boundary layer height and moisture  
41 conditions (Shi et al., 2019; Niu et al., 2010; Ding et al., 2014). During December 16th-21st 2016, although most aggressive  
42 control measures for anthropogenic emissions were implemented, severe haze pollution with PM<sub>2.5</sub> concentrations  $\approx 1100\mu\text{g}$   
43  $\text{m}^{-3}$  still occurred and covered 710,000km<sup>2</sup>. The continuous low surface wind speed of less than 2ms<sup>-1</sup>, high humidity above  
44 80% and strong temperature inversion lasting for 132h caused the serious haze event in 2016 (Yin and Wang, 2017). In winter  
45 2017, the air quality in North China largely improved; however, the stagnant atmosphere in 2018 resulted in a major PM<sub>2.5</sub>  
46 rebound comparing to 2017 by weakening transport dispersion and enhancing the chemical production of secondary aerosols  
47 (Yin and Zhang 2020). Wang et al. (2020) applied the Community Multiscale Air Quality model to emphasize that the role of  
48 adverse meteorological conditions cannot be neglected even during the COVID-19 outbreak. From February 8 to 13 2020,  
49 North China suffered severe pollutions, with maximum daily PM<sub>2.5</sub> exceeding 200 $\mu\text{g m}^{-3}$ . During this period, weak southerly  
50 surface winds lasted for nearly 5 days, relative humidity was close to 100%, and atmospheric inversion reached more than  
51 10°C. Although pollution emissions from basic social activities have been reduced, heavy pollution still occurred when adverse  
52 meteorological conditions characterized by stable air masses appeared (Wang et al., 2020).

53 After the severe haze events of 2013, routine emission reductions resulted in an approximately 42% decrease in the annual  
54 mean PM<sub>2.5</sub> concentration between 2013 and 2018 in China (Cleaner air for China, 2019). In November 2019, the Ministry of  
55 Environmental Protection of China issued a series of Autumn-Winter Air Pollution Prevention and Management Plans  
56 indicating that the routine emission reductions would be conventionally implemented in the following winter (Ministry of  
57 Environmental Protection of China, 2019). As reported by the government, the mean ratio of work resumption in large  
58 industrial enterprises was approximately 90% in the east of China until the end of February (Fig. 1b). In this study, we attempted  
59 to quantify the impacts of the COVID-19 pandemic on the observed PM<sub>2.5</sub> concentration in February 2020 when the quarantine  
60 measures were the strictest. The official 7-day Chinese New Year holiday occurs in January and February and commonly  
61 accounts for approximately 25% of a month. From 2013–2020, there were only two years (2017 and 2020) when the official  
62 7-day holiday occurred in January (Fig. 1c). Thus, to avoid the impacts of the Spring Festival, the observed PM<sub>2.5</sub> concentration

63 in February 2017 (Fig. 1a) was adopted to calculate the PM<sub>2.5</sub> difference, which was decomposed into the results due to  
64 expected routine emission reductions, changing meteorology climate variability, and COVID-19 quarantines.

65 **2 Datasets and methods**

66 **2.1 Data description**

67 Monthly mean meteorological data from 2015 to 2020 were obtained from NCEP/NCAR reanalysis datasets, with a  
68 horizontal resolution of 2.5°×2.5°, including the geopotential height at 500 hPa (H500), zonal and meridional winds at 850  
69 hPa, vertical wind from the surface to 150 hPa, and relative humidity at the surface (Kalnay et al., 1996). PM<sub>2.5</sub> concentration  
70 data from 2015 to 2020 were acquired from the China National Environmental Monitoring Centre (<https://quotsoft.net/air/> ).  
71 The monitoring network expanded from 1500 sites in 2015 to 1640 sites in 2020, covering approximately 370 cities nationwide.  
72 The PM<sub>2.5</sub> data were monitored every 5 min using two methods: a tapered element oscillating microbalance and β-rays, which  
73 were operated under the China National Quality Control.

74 **2.2 GEOS-Chem description, evaluation and experimental design.**

75 We used the GEOS-Chem model (<http://acmg.seas.harvard.edu/geos/>) to simulate the PM<sub>2.5</sub> concentration, driven by  
76 MERRA-2 assimilated meteorological data (Gelaro et al., 2017). The nested grid over China (15° N–55° N, 75–135° E) had a  
77 horizontal resolution of 0.5° latitude by 0.625° longitude and consisted of 47 vertical layers up to 0.01 hPa. The GEOS-Chem  
78 model included the fully coupled O<sub>3</sub>–NO<sub>x</sub>–hydrocarbon and aerosol chemistry module with more than 80 species and 300  
79 reactions (Bey et al., 2001; Park et al., 2004). The PM<sub>2.5</sub> components simulated in the GEOS-Chem model included sulfate,  
80 nitrate, ammonium, black carbon and primary organic carbon, mineral dust, and sea salt. Aerosol thermodynamic equilibrium  
81 is computed by the ISORROPIA package, which calculates the gas–aerosol partitioning of the sulfate–nitrate–ammonium  
82 system (Fountoukis and Nenes, 2007). Heterogeneous reactions of aerosols include the uptake of HO<sub>2</sub> by aerosols (Thornton  
83 et al., 2008), irreversible absorption of NO<sub>2</sub> and NO<sub>3</sub> on wet aerosols (Jacob, 2000), and hydrolysis of N<sub>2</sub>O<sub>5</sub> (Evans and Jacob,  
84 2005). Two alternate simulations of aerosol microphysics are implemented in GEOS-Chem: the TOMAS simulation (Kodros  
85 and Pierce, 2017) and the APM simulation (Yu and Luo, 2009), which were both simulated in the experiments.

86 GEOS-Chem model has been widely used to examine the historical changes in air quality in China and quantitatively  
87 separate the impacts of physical-chemical processes. Using the GEOS-Chem model, Yang et al. (2016) found an increasing  
88 trend of winter PM<sub>2.5</sub> concentrations during 1985–2005, 80% of which due to anthropogenic emissions and 20% due to  
89 meteorological conditions. Here, we simulated the PM<sub>2.5</sub> concentrations in February 2017 and evaluated the performance of  
90 GEOS-Chem (Fig. 2a). The values of mean square error / mean equals were 5.8%, 7.0% and 5.4% in North China (NC),  
91 Yangtze River Delta (YRD) and Hubei Province (HB), respectively, indicating the good performance of reproducing the haze-

92 polluted conditions. The absolute biases were larger in the south of China, which was consistent with Dang and Liao (2019).  
93 They also compared the simulated and observed daily mean  $PM_{2.5}$  concentrations at the Beijing, Shanghai, and Chengdu grids,  
94 which had a low bias in Beijing with a normalized mean bias (NMB) of -9.2% and high biases with NMBs of 18.6% and 28.7%  
95 in Shanghai and Chengdu, respectively. The simulations in February 2017 in this study substantially underestimated the  $PM_{2.5}$   
96 in NC with an NMB of -3.0% (Fig. 2a). Among them, the NMB in The Beijing-Tianjin-Hebei region was -3.3%. However, in  
97 the Fenwei plain, the underestimation was even more pronounced, with NMB reaching -16.3%. The simulated biases possibly  
98 affected the subsequent results and brought uncertainties to some extent. The simulated spatial distribution of  $PM_{2.5}$  was also  
99 similar to that of observations with spatial correlation coefficient = 0.78.

100 We further verified whether the simulations could capture the roles of meteorological changes in February 2020 under a  
101 substantial reduction in emissions because of COVID-19 quarantines. In NC, YRD and HB, the correlation coefficients  
102 between daily  $PM_{2.5}$  observations and simulated data under 2010 (1985) emission scenario reached 0.83 (0.82), 0.67 (0.63),  
103 and 0.79 (0.73), respectively (Fig. 2b-d), and could capture the maximum and minimum  $PM_{2.5}$  concentrations. For example,  
104 in NC, the simulation could well simulate severe haze events (e.g., from 8–13 and 19–25 February) and good air quality events  
105 (e.g., from 14–18 February), reflecting that it has ability to accurately capture the change of meteorological conditions. The  
106 correlation coefficients under 2010 emission scenario were all higher than that under 1985 emission scenario maybe due to the  
107 emissions from each sector in 2010 were more similar to recent years, which was more reasonable.

108 The  $PM_{2.5}$  concentration in February from 2015 to 2020 was simulated in this study. Due to delayed updates of the  
109 emission inventory, we used the emissions data of 2010  
110 (<http://geoschemdata.computeCanada.ca/ExtData/HEMCO/AnnualScalar>) and 1985 (M. Li et al., 2017) for the simulations,  
111 which represented high- and low-emission scenarios, respectively. In total, we conducted two sets of numerical experiments  
112 to drive the GEOS-Chem simulations, one combining the meteorological conditions from 2015 to 2020 with fixed emissions  
113 in 1985 and the other with fixed emissions in 2010, which could determine the stability of simulated results.

### 114 2.3 The method to quantify the influence of the COVID-19 quarantine.

115 As mentioned above, we aimed to examine the impact of the COVID-19 quarantines on  $PM_{2.5}$  over the February 2017  
116 level basing on an observational-numerical hybrid method. The observed  $PM_{2.5}$  difference in February 2020 ( $PM_{2.5}^{OBS}$ ) was  
117 linearly decomposed into three parts: the impacts of changing meteorology ( $PM_{dM}$ ), expected routine emissions reductions  
118 ( $PM_{dR}$ ) and COVID-19 quarantines ( $PM_{dC}$ ), which was a reasonable approximation, and the decomposition equation was  
119  $PM_{2.5}^{OBS} = PM_{dM} + PM_{dR} + PM_{dC}$ . That is,  $PM_{dC} = PM_{2.5}^{OBS} - PM_{dM} - PM_{dR}$ . It should be noted that  $PM_{dC}$  is the impact of  
120 the COVID-19 quarantines over the situation whereby the pandemic did not occur and routine emission reductions  
121 conventionally were in effect. The value of  $PM_{dE}$  (i.e.,  $PM_{dR} + PM_{dC}$ ) was the total impact of the emission reductions in  
122 February 2020 over the 2017 level.

123 Simulated PM<sub>2.5</sub> data driven by changing meteorology with two fixed-emissions (1985 and 2010) were employed to  
124 determine the ratio of PMd<sub>M</sub> of each year/ observed PM<sub>2.5</sub> in 2017. Depending on the GEOS-Chem simulations, we found that  
125 the percentage of changed PM<sub>2.5</sub> due to the differences in meteorology remained nearly constant regardless of the emission  
126 level (Fig. S1), which was consistent with the results of Yin and Zhang (2020). This percentage was the difference of simulated  
127 PM<sub>2.5</sub> between each year and 2017 under the same emission scenario divided by the simulated PM<sub>2.5</sub> in 2017. For example, the  
128 percentages due to different meteorology between 2020 and 2017 were 22.1% (21.4%), -1.2% (-0.7%) and 9.0% (8.2%) in  
129 NC, YRD and HB under the low (high) emissions (Fig. S1). The percentage under 2010 emission scenario was selected as the  
130 final percentage because the emissions from each sector in 2010 were more similar to recent years, and thus was more  
131 reasonable. Then, through multiplying the 2017 observation by this percentage, PMd<sub>M</sub> can be quantified in each simulation  
132 grid with respect to 2017 (STEP 1).

133 From 2015 to 2019, PMd<sub>C</sub> = 0; thus, PMd<sub>R</sub> = PMd<sub>OBS</sub> – PMd<sub>M</sub>. Here, we repeated STEP 1 to determine PMd<sub>M</sub> in each year  
134 from 2015 to 2019 relative to 2017 (i.e., PMd<sub>M</sub> = 0 in 2017). After removing the effect of meteorological conditions in PM<sub>2.5</sub>  
135 differences, PMd<sub>R</sub> in all years except 2020 can also be calculated. According to many previous studies, the change in emissions  
136 resulted in a linear change in air pollution in China from 2013-2019 (Wang et al., 2020; Geng et al., 2020) which might be  
137 related to the huge emission reduction due to the implementation of clean air action. Because the signal of emissions reduction  
138 in China had been particularly strong since 2013, it could be easily detected and the assumption of a linear reduction in  
139 pollution caused by emission reduction was applicable in China in the past few years. Based on this approximation, we used  
140 the method of extrapolation to speculate the impact of routine emission reduction on PM<sub>2.5</sub>. We performed linear extrapolation  
141 based on known PMd<sub>R</sub> values from 2015 to 2019 to obtain PMd<sub>R</sub> in 2020 (STEP 2, Fig. S2). This PMd<sub>R</sub> in 2020 was calculated  
142 as the change of PM<sub>2.5</sub> caused by expected routine emission reduction, which did not actually happen, but merely gave an  
143 assessment in the case of “if no COVID-19”. In Beijing and Shanghai, for example, PM<sub>2.5</sub> fell by 23.1% and 26.6% due to  
144 routine emission reduction in 2019, respectively, compared with 2015. Zhou et al. (2020) indicated that emission reductions  
145 caused 20–26% decreases in winter in Beijing which has been translated into 5 years. Zhang et al. (2020) also showed that the  
146 emission controls in Beijing-Tianjin-Hebei (BTH) region have led to significant reductions in PM<sub>2.5</sub> from 2013 to 2017 of  
147 approximately 20 % after excluding the impacts of meteorology. Geng et al. (2020) found a 20% drop in the main component  
148 of PM<sub>2.5</sub> in the Yangtze River Delta from 2013 to 2017. These results are consistent with our extrapolated results. Therefore,  
149 it is reasonable to obtain PMd<sub>R</sub> by extrapolation after disentangling the effects of meteorological conditions.

150 Through STEP 1 and STEP 2, PMd<sub>C</sub> and PMd<sub>R</sub>, respectively, in 2020 can be determined. PMd<sub>OBS</sub> can be directly  
151 calculated from the observed data. After removing the influences of climate anomalies and routine emission reductions, the  
152 impact of COVID-19 quarantines on PM<sub>2.5</sub> (PMd<sub>C</sub>) was extracted as PMd<sub>OBS</sub> – PMd<sub>M</sub> – PMd<sub>R</sub> (STEP 3).

153 **3 Results**

154 The mean  $\text{PM}_{2.5}$  concentration in February 2020 was nearly below  $80 \text{ }\mu\text{g}/\text{m}^3$  at the vast majority of sites in the east of  
155 China, which was much lower than before (Fig. S3). North China (NC) was still the most polluted region ( $>40 \text{ }\mu\text{g}/\text{m}^3$ ), but the  
156  $\text{PM}_{2.5}$  concentrations in the Pearl River Delta (PRD) and Yangtze River Delta (YRD) were  $< 20 \text{ }\mu\text{g}/\text{m}^3$  and  $< 40 \text{ }\mu\text{g}/\text{m}^3$ ,  
157 respectively. Relative to the observations in February 2017, negative  $\text{PM}_{2.5}$  anomalies were centered in NC, with values of  
158 approximately  $-60$  to  $-40 \text{ }\mu\text{g}/\text{m}^3$  in southern Hebei Province and northern Henan Province (Fig. 3). In Hubei Province (HB),  
159 where the COVID-19 pneumonia cases were the most severe in February, the  $\text{PM}_{2.5}$  concentration was  $20\text{--}40 \text{ }\mu\text{g}/\text{m}^3$  lower  
160 than that in 2017. The  $\text{PM}_{2.5}$  differences were also negative in YRD and PRD. Therefore, how much did air pollution decrease  
161 due to the COVID-19 quarantines in February in east of China?

162 Climate variability notably influences the interannual-decadal variations in haze pollution as verified by both  
163 observational analysis (Yin et al., 2015) and GEOS-Chem simulations (Dang and Liao, 2019). Furthermore, Zhang et al. (2020)  
164 reported that meteorology contributes 50% and 78% of the wintertime  $\text{PM}_{2.5}$  reduction between 2017 and 2013 in the BTH  
165 and YRD, respectively. Therefore, it is necessary to disentangle the influences of climate anomalies before quantifying the  
166 contributions of the COVID-19 quarantines on the air quality. The highest observed  $\text{PM}_{2.5}$  concentrations were 274, 223, and  
167  $303 \text{ }\mu\text{g}/\text{m}^3$  in Beijing, Tianjin and Shijiazhuang, respectively. Although human activities had sharply decreased, severe haze  
168 pollution (e.g., 8–13 and 19–25 February 2020) was not avoided, which was attributed to the stagnant atmosphere (Wang et  
169 al., 2020), and these severe haze events were also reproduced by the GEOS-Chem simulation (see Section 2.2 and Fig. 2b).

170 As shown in Figure 4a-b, the meteorological conditions in February 2020 were more favorable for the occurrence of haze  
171 pollution in NC. In the mid-troposphere, an anomalous anticyclone was located over NC and the Sea of Japan (Fig. 4a). These  
172 anticyclonic anomalies clearly stimulated anomalous southerlies over eastern China, which not only transported sufficient  
173 water vapor to NC but also overwhelmed the climatic northerlies in winter (Fig. 4b). In addition, the anomalous upward motion  
174 associated with anomalous anticyclones prevented the downward transportation of westerly momentum and preserved the  
175 thermal inversion layer over NC (Fig. S4). Particularly, in the stagnant days (i.e., 8–13 and 19–25 February), the East Asia  
176 deep trough, one of the most significant zonally asymmetric circulations in the wintertime Northern Hemisphere (Song et al.,  
177 2016), shifted eastwards and northwards than climate mean, which steered the cold air to North Pacific instead of North China  
178 (Fig. 4c). The climatic northerlies in February, related to East Asia winter monsoon, also turned to be south winds in the east  
179 of China (Fig. 4d). Physically, the weakening surface winds and strong thermal inversion corresponded to weaker dispersion  
180 conditions, and the higher humidity indicated a favorable environment for the hygroscopic growth of aerosol particles to  
181 evidently decrease the visibility. Compared with the climate (February 2017) monthly mean, boundary layer height (BLH)  
182 decreased by 19.5m (34.5m), surface relative humidity (rhum) increased by 5% (10.6%) and surface air temperature (SAT)  
183 rose by  $1.6^\circ\text{C}$  ( $0.9^\circ\text{C}$ ) after detrending, which were conducive to the increase of  $\text{PM}_{2.5}$  concentration in February 2020.

184 Furthermore, the correlation coefficients of daily  $\text{PM}_{2.5}$  and BLH, rhum, wind speed and SAT in North China were -0.63, 0.44,  
185 -0.45 and 0.46, respectively, all of which passed the 95% significance test using *t* test method and indicated importance of  
186 meteorology. We used the meteorological data in February 2017 to establish a multiple linear regression equation to fit  $\text{PM}_{2.5}$ .  
187 The correlation coefficients between the fitting results and the observed  $\text{PM}_{2.5}$  concentration in NC, YRD and HB reached 0.84,  
188 0.64 and 0.65, exceeding the 99% significance test using *t* test method. Then, we put the observed meteorological data in  
189 February 2020 into this established multiple regression equation to get the predicted  $\text{PM}_{2.5}$  concentration. Using the regress-  
190 predicted value, the percentage of changed  $\text{PM}_{2.5}$  due to the differences in meteorology between 2017 and 2020 were re-  
191 calculated and is 20.7%, -3.2% and 9.5% in NC, YRD and HB, respectively (Fig. S1), which is consistent with and enhanced  
192 the robustness of the results obtained by our previous model simulation. Based on the GEOS-Chem simulations,  $\text{PMd}_M$  was  
193 calculated between February 2020 and 2017 (see Methods). To the south of 30°N, most  $\text{PMd}_M$  values were negative with small  
194 absolute values, at  $< 10 \mu\text{g}/\text{m}^3$ . To the north of 30°N, the  $\text{PMd}_M$  values were mostly positive, ranging from 30~60  $\mu\text{g}/\text{m}^3$  in  
195 BTH (Fig. 5a).

196 Since 2013, the Chinese government has legislated and implemented stringent air pollution prevention and management  
197 policies that have clearly contributed to air quality improvement (Wang et al., 2019). As mentioned above, without the COVID-  
198 19 pandemic, these emission reduction policies would certainly remain in effect in February 2020. Thus, we extrapolated  $\text{PMd}_R$   
199 (i.e., the  $\text{PM}_{2.5}$  difference due to expected routine emission reductions) between February 2020 and 2017 to isolate the impacts  
200 of the COVID-19 quarantines (i.e.,  $\text{PMd}_C$ ).  $\text{PMd}_R$  was mostly negative in the east of China (Fig. 5b). Because the impacts of  
201 meteorology were proactively removed, these negative values illustrated that routine emission reductions substantially reduced  
202 the wintertime  $\text{PM}_{2.5}$  concentration. The contributions of the emission reduction policies were the greatest in the south of BTH  
203 and were also remarkable in Hubei Province (Fig. 5b). Although the  $\text{PMd}_R$  of Beijing in 2016 did not strictly comply with the  
204 pattern of monotonous decrease, which might be caused by the fluctuation of policy and its implementation, the value of  $\text{PMd}_R$   
205 in 2020 relative to 2017 was  $-8.4 \mu\text{g}/\text{m}^3$  and was comparable to the  $11.5 \mu\text{g}/\text{m}^3$  reductions due to policy during 2013–2017  
206 (Zhang et al., 2020). In Shanghai,  $\text{PMd}_R$  was  $-12.0 \mu\text{g}/\text{m}^3$  (Fig. 6), whose magnitude was proportional with assessments by  
207 Zhang et al. (2020), and the trend was nearly linear. The rationality of the extrapolations of  $\text{PMd}_R$  was also proved in Section  
208 2.3. The trend of  $\text{PMd}_R$  in Wuhan was  $-9.6 \mu\text{g}/\text{m}^3$  per year from 2015–2019, which indicated high efficiency of the emission  
209 reduction policies and resulted in large  $\text{PMd}_R$  values in 2020 (i.e.,  $-21.8 \mu\text{g}/\text{m}^3$ ).

210 By disentangling the impacts of meteorology and routine emission reduction policies, the change in  $\text{PM}_{2.5}$  due to the  
211 COVID-19 quarantines was quantitatively extracted. As expected, this severe pandemic caused dramatic slumps in the  $\text{PM}_{2.5}$   
212 concentration across China (Fig. 5c). Large  $\text{PMd}_C$  values (approximately  $-60$  to  $-30 \mu\text{g}/\text{m}^3$ ) were located in the high-polluted  
213 NC regions where intensive heavy industries were stopped and the traditional massive social activities and transportations  
214 around Chinese New Year were cancelled as part of the COVID-19 quarantine measures. To the south of 30°N, the impacts of  
215 the COVID-19 quarantines on the air quality were relatively weaker ( $-30 \sim 0 \mu\text{g}/\text{m}^3$ ) than those in the north. Generally, the

south region was less polluted than the north, therefore the baseline of  $\text{PM}_{2.5}$  concentration was relatively lower (Fig. S3a). In addition, meteorological conditions in the south in February 2020 had no positive contribution (Fig. 5a), which would not lead to the increase of  $\text{PM}_{2.5}$  concentration. These two possible reasons resulted in a smaller space for  $\text{PM}_{2.5}$  decrease due to COVID-19 quarantines in the south and accompanying regional differences. To reduce the assessment uncertainties, the percentage of changed  $\text{PM}_{2.5}$  due to the differences in meteorology were recalculated based on the GEOS-Chem simulations with fixed emission in 1985. As described in the Methods section, the recalculated  $\text{PM}_{\text{dC}}$  in Figure S5 were consistent with those in Figure 5c, showing a high robustness. Furthermore, the mean  $\text{PM}_{2.5}$  concentration decreases due to the COVID-19 quarantines in NC, HB and YRD were analyzed, which accounted for 59%, 26% and 72% of the observed February  $\text{PM}_{2.5}$  concentration in 2020 (Fig. 7).

It should be noted that the sum of  $\text{PM}_{\text{dR}}$  and  $\text{PM}_{\text{dC}}$  (i.e.,  $\text{PM}_{\text{dE}}$ ) is the total contribution of the emission reduction in February 2020 with respect to 2017 (Fig. 5d). In NC, YRD and HB, the COVID-19 quarantines and routine emission reductions drove  $\text{PM}_{2.5}$  in the same direction. The mean  $\text{PM}_{2.5}$  decrease in NC, due to the total emission reduction, was  $-43.3 \mu\text{g}/\text{m}^3$ , accounting for 79% of the observed February  $\text{PM}_{2.5}$  concentration in 2020 (Fig. 7). Although the absolute values of both  $\text{PM}_{\text{dR}}$  and  $\text{PM}_{\text{dC}}$  in YRD were smaller than those in NC, the change percentage (92%) was larger because of the lower base  $\text{PM}_{2.5}$  concentration. In HB, where more than 80% of the confirmed COVID-19 cases in China occurred and the cities were in emergency lockdown, the total anthropogenic emissions were clearly limited, which resulted in a 72% decline in  $\text{PM}_{2.5}$  in the atmosphere (Fig. 7). In particular, if the anthropogenic emissions did not decline, the  $\text{PM}_{2.5}$  concentration in NC, YRD and HB would increase to nearly twice the current observation (Fig. 7), indicating significant contributions of human activities to the air pollution in China.

The declines of  $\text{PM}_{2.5}$  seemed not to be directly proportional to the almost complete shutoff of vehicle traffics and industries, that is, the reduction ratio of  $\text{PM}_{2.5}$  concentrations were smaller than that of precursor emissions (Wang et al., 2020). The unexpected air pollutions during the marked emission reductions were closely related to the stagnant air flow, enhanced productions of secondary aerosols, and uninterrupted residential heating, power plants and petrochemical facilities (Le et al., 2020). The partial impacts of stagnant meteorological conditions have been explained earlier (Fig. 4). In Wuhan, the  $\text{PM}_{2.5}$  remained the main pollutant during the city lockdown and the high level of sulphur dioxide ( $\text{SO}_2$ ) may be related to the increased domestic heating and cooking (Lian et al., 2020). In North China, large reductions of primary aerosols were observed, but the decreases in secondary aerosols were much smaller (Sun et al., 2020; Shi et al., 2020). Because of the disruption of transportations, reduced nitrogen oxide ( $\text{NO}_x$ ) increased the concentrations of ozone and nighttime nitrate ( $\text{NO}_3^-$ ) radical formations. The increased oxidizing capacity in the atmosphere enhanced the formation of secondary particulate matters (Huang et al., 2020). Thus, the non-linear relationship of emission reduction and secondary aerosols also partially contributed to the haze occurrence during the COVID-19 lockdown.

247 **4 Conclusions and discussion**

248 In the beginning of 2020, the Chinese government implemented top-level emergency response measures to contain the  
249 spread of COVID-19. The traditional social activities surrounding Chinese New Year, industrial and transportation activities,  
250 etc. were prohibited, which effectively reduced the number of confirmed cases in China. Concomitantly, anthropogenic  
251 emissions, which are the fundamental reason for haze pollution, were dramatically reduced by the COVID-19 quarantine  
252 measures. In this study, we employed observations and GEOS-Chem simulations to quantify the impacts of the COVID-19  
253 quarantines on the air quality improvement in February 2020 after decomposing the contributions of expected routine emission  
254 reductions and climate variability. Although the specific influences varied by the region, the COVID-19 quarantines  
255 substantially decreased the level of haze pollution in the east of China (Fig. 7). In North China, the meteorological conditions  
256 were stagnant that enhanced the  $PM_{2.5}$  concentration by 30% (relative to the observations in 2020). In contrast, the expected  
257 routine emissions reductions and emergency COVID-19 quarantine measures resulted in an 80% decline. In YRD, the impacts  
258 of meteorology were negligible but the COVID-19 quarantines decreased  $PM_{2.5}$  by 72%. In Hubei Province, the impact of the  
259 total emission reduction (72%) evidently exceeded the  $PM_{2.5}$  increase due to meteorological conditions (13%). In March, due  
260 to the continued control of the COVID-19, the quarantines measures still contributed to the negative anomalies of the observed  
261  $PM_{2.5}$  between 2020 and 2017 (Fig. 8a). Because the activities in production and life have been gradually resumed in March,  
262 the  $PM_{2.5}$  drops caused by the COVID-19 quarantines became weaker compared with February (Fig. 8b, c). The contributions  
263 of  $PM_{dC}$  to the change of  $PM_{2.5}$  concentration in NC, YRD and HB declined from 32.2, 21.0 and 12.1  $\mu g/m^3$  in February to  
264 7.0, 2.4 and 6.7  $\mu g/m^3$  in March respectively.

265 Because of the common update delay of the emission inventory, we employed a combined analysis consisting of  
266 observational and numerical methods. We strictly demonstrated the rationality of this method and the results, mainly based on  
267 the relatively constant contribution ratio of changing meteorology from GEOS-Chem simulations under the different emissions  
268 (Yin and Zhang 2020). However, there was a certain bias in the simulations by GEOS-Chem model, and the biases also showed  
269 regional differences (Dang and Liao, 2019). Therefore, gaps between the assessed results and reality still exist, which requires  
270 further numerical experiments when the emission inventory is updated. Furthermore, during the calculation process, the  
271 observed  $PM_{2.5}$  difference in February 2020 was linearly decomposed into three parts. Although this linear decomposition was  
272 reasonable in China in the past few years, we must note that this approximation did not consider the meteorology-emission  
273 interactions, the product of the emission, the loss lifetime and particularly the sulfate-nitrate-ammonia thermodynamics (Cai  
274 et al., 2017), which brought some uncertainties. The actual emission reduction effect is considerable (Fig. 3d), in line with the  
275 increasingly strengthened emission reduction policies in recent years. When calculating the  $PM_{dR}$  in 2020, we use the method  
276 of extrapolation. Although the result is consistent with others observational and numerical studies (Geng et al., 2020; Zhang  
277 et al., 2020; Zhou et al., 2019), it is still estimated value rather than true value. These issues need to be examined in the future

278 studies to unlock respective effects of emissions and meteorological conditions on PM<sub>2.5</sub> over eastern China. To restrict the  
279 possible uncertainties, we set up some constraints: 1. The pivotal contribution ratio of changing meteorology were calculated  
280 under two emission levels and recalculated by statistical regressed model; 2. The values of PM<sub>dM</sub> and PM<sub>dr</sub> were widely  
281 compared to previous studies.

282 If the COVID-19 epidemic did not occurred, the concentrations of PM<sub>2.5</sub> would increase up to 1.3–1.7 times the  
283 observations in February 2020 (Fig. 7). Therefore, the pollution abatement must continue. Because of the huge population base  
284 in the east of China, the anthropogenic emissions exceeded the atmospheric environmental capacity even during COVID-19  
285 quarantines. Although the PM<sub>2.5</sub> dropped much, marked air pollutions also occurred during this unique experiments that the  
286 human emissions were sharply closed. This raised new scientific questions, such as changes of atmospheric heterogeneous  
287 reactions and oxidability under extreme emission control, quantitative meteorology-emission interactions, and so on. This also  
288 implied reconsiderations of policy for pollution controls and necessity to cut off secondary productions of particulate matters  
289 basing on sufficient scientific research (Le et al., 2020; Huang et al., 2020). Some studies estimated that thousands of deaths  
290 were prevented during the quarantine because of the air pollution decrease (Chen K. et al., 2020). However, medical systems  
291 were still overstressed, and transportation to hospitals also decreased. Furthermore, the deaths related to air pollution were  
292 almost all due to respiratory diseases (Wang et al., 2001), and their corresponding medical resources were also further stressed  
293 by COVID-19. Therefore, the mortality impacted by the air pollution reduction during the COVID-19 outbreak should be  
294 comprehensively assessed in future work.

295 **Data availability.** Monthly mean meteorological data are obtained from ERA5 reanalysis data archive:  
296 <https://cds.climate.copernicus.eu/cdsapp#!/search?type=dataset>. PM<sub>2.5</sub> concentration data are acquired from the China  
297 National Environmental Monitoring Centre: <http://beijingair.sinaapp.com/>. The emissions data of 1985 can be downloaded  
298 from <http://geoschemdata.computechina.ca/ExtData/HEMCO/AnnualScalar/>, and that of 2010 can be obtained from MIX:  
299 <http://geoschemdata.computechina.ca/ExtData/HEMCO/MIX>.

### 300 **Acknowledgements**

301 The National Natural Science Foundation of China (42088101, 41991283, 9174431 and 41705058) and the special project  
302 “the impacts of meteorology on large-scale spread of influenza virus” from CIC-FEMD supported this research.

### 303 **Authors' contribution**

304 Wang H. J. and Yin Z. C. designed and performed researches. Zhang Y. J. simulated the PM<sub>2.5</sub> by GEOS-Chem model and Li  
305 Y. Y. did the statistical analysis. Yin Z. C. prepared the manuscript with contributions from all co-authors.

### 306 **Competing interests**

307 The authors declare no conflict of interest.

309 Bey, I., Jacob, D. J., Yantosca, R. M., Logan, J. A., Field, B. D., Fiore, A. M., Li, Q. B., Liu, H. G. Y., Mickley, L. J., and  
310 Schultz, M. G.: Global modeling of tropospheric chemistry with assimilated meteorology: Model description and evaluation,  
311 *J. Geophys. Res. Atmos.*, 106, 23073–23095, <https://doi.org/10.1029/2001jd000807>, 2001.

312 Cai, S., Wang, Y., Zhao, B., Wang S., Chang, X., and Hao, J.: The impact of the “Air Pollution Prevention and Control Action  
313 Plan” on PM<sub>2.5</sub> concentrations in Jing-Jin-Ji region during 2012–2020, *Sci. Total Environ.*, 580, 197 –209, 2017.

314 Cao, W., Fang, Z., Hou, G., Han, M., Xu X., and Dong, J.: The psychological impact of the COVID-19 epidemic on college  
315 students in China, *Psychiat. Res.*, 287, 112934, 2020.

316 Chen, S., Yang, J., Yang W., Wang, C., and Till, B.: COVID-19 control in China during mass population movements at New  
317 Year, *Lancet*, 395(10226), 764–766, 2020.

318 Chen, K., Wang, M., Huang, C., Patrick, L., and Paul, T.: Air Pollution Reduction and Mortality Benefit during the COVID-  
319 19 Outbreak in China, *MedRxiv*, <https://doi.org/10.1101/2020.03.23.20039842>, 2020.

320 Cleaner air for China, *Nat. Geosci.*, 12, 497–497, <https://doi.org/10.1038/s41561-019-0406-7>, 2019.

321 Dang, R., and Liao, H.: Severe winter haze days in the Beijing-Tianjin-Hebei region from 1985 to 2017 and the roles of  
322 anthropogenic emissions and meteorology, *Atmos. Chem. Phys.*, 19, 10801–10816, 2019.

323 Ding, Y., and Liu, Y.: Analysis of long-term variations of fog and haze in China in recent 50 years and their relations with  
324 atmospheric humidity, *Sci. China Ser. D.*, 57, 36–46, 2014.

325 Evans, M. J. and Jacob, D. J.: Impact of new laboratory studies of N<sub>2</sub>O<sub>5</sub> hydrolysis on global model budgets of  
326 tropospheric nitrogen oxides, ozone, and OH, *Geophys. Res. Lett.*, 32, L09813, <https://doi.org/10.1029/2005gl022469>,  
327 2005.

328 Fountoukis, C. and Nenes, A.: ISORROPIA II: a computationally efficient thermodynamic equilibrium model for K<sup>+</sup>-  
329 Ca<sup>2+</sup>-Mg<sup>2+</sup>-NH<sub>4</sub><sup>+</sup>-Na<sup>+</sup>-SO<sub>4</sub><sup>2-</sup>-NO<sub>3</sub><sup>-</sup>-Cl<sup>-</sup>-H<sub>2</sub>O aerosols, *Atmos. Chem. Phys.*, 7, 4639–4659, <https://doi.org/10.5194/acp-7-4639-2007>, 2007.

330 Gelaro, R., McCarty, W., Suarez, M. J., Todling, R., Molod, A., Takacs,L., Randles,C.A., Darmenov,A., Bosilovich,M.G.,  
331 Reichle, R., Wargan, K., Coy, L., Cullather, R., Draper, C., Akella, S., Buchard, V., Conaty, A., da Silva, A. M., Gu, W., Kim,  
332 G. K., Koster, R., Lucchesi, R., Merkova, D., Nielsen, J. E., Partyka,G., Pawson,S., Putman,W., Rienecker,M., Schubert,S.D.,  
333 Sienkiewicz, M., and Zhao, B.: The Modern-Era Retrospective Analysis for Research and Applications, Version 2 (MERRA2),  
334 *J. Climate*, 30, 5419–5454, <https://doi.org/10.1175/jcli-d-160758.1>, 2017.

335 Geng, G., Xiao, Q., Zheng, Y., Tong, D., Zhang, Y., Zhang, X., Zhang, Q., He, H., and Liu, Y.: Impact of China’s Air Pollution  
336 Prevention and Control Action Plan on PM<sub>2.5</sub> chemical composition over eastern China, *Sci. China Ser. D.*, 62, 1872–1884,  
337 <https://doi.org/10.1007/s11430-018-9353-x>, 2020.

339 Huang, X., Ding, A., Gao, J., Zheng, B., Zhou, D., Qi, X., Tang, R., Ren, C., Nie, W., Chi, X., Wang, J., Xu, Z., Chen, L., Li,  
340 Y., Che, F., Pang, N., Wang, H., Tong, D., Qin, W., Cheng, W., Liu, W., Fu, Q., Chai, F., Davis, S., Zhang, Q., and He, K.:  
341 Enhanced secondary pollution offset reduction of primary emissions during COVID-19 lockdown in China, *Natl. Sci. Rev.*,  
342 nwaa 137, 2020.

343 Jacob, D. J.: Heterogeneous chemistry and tropospheric ozone, *Atmos. Environ.*, 34, 2131–2159,  
344 [https://doi.org/10.1016/s1352-2310\(99\)00462-8](https://doi.org/10.1016/s1352-2310(99)00462-8), 2000.

345 Kalnay, E., Kanamitsu, M., Kistler, R., Collins, W., Deaven, D., Gandin, L., Iredell, M., Saha, S., White, G., Woollen, J., Zhu,  
346 Y., Leetmaa, A., Reynolds, R., Chelliah, M., Ebisuzaki, W., Higgins, W., Janowiak, J., Mo, K. C., Ropelewski, C., Wang, J.,  
347 Jenne, R., and Joseph, D.: The NCEP/NCAR 40-year reanalysis project, *B. Am. Meteorol. Soc.*, 77, 437–471,  
348 [https://doi.org/10.1175/1520-0477\(1996\)077<0437:TNYRP>2.0.CO;2](https://doi.org/10.1175/1520-0477(1996)077<0437:TNYRP>2.0.CO;2), 1996.

349 Kodros, J. K., Pierce, J. R.: Important global and regional differences in cloud-albedo aerosol indirect effect estimates between  
350 simulations with and without prognostic aerosol microphysics, *J. Geophys. Res.*, 122, <https://10.1002/2016JD025886>, 2017.

351 Le, T., Wang, Y., Liu, L., Yang, J., Yung, Y. L., Li, G., and John, H.: Unexpected air pollution with marked emission reductions  
352 during the covid-19 outbreak in China, *Science*, 369(6504), eabb7431, 2020.

353 Li, M., Zhang, Q., Kurokawa, J.-I., Woo, J.-H., He, K., Lu, Z., Ohara, T., Song, Y., Streets, D. G., Carmichael, G. R., Cheng,  
354 Y., Hong, C., Huo, H., Jiang, X., Kang, S., Liu, F., Su, H., and Zheng, B.: MIX: a mosaic Asian anthropogenic emission  
355 inventory under the international collaboration framework of the MICS-Asia and HTAP, *Atmos. Chem. Phys.*, 17, 935–963,  
356 <https://doi.org/10.5194/acp-17-935-2017>, 2017.

357 Lian, X., Huang, J., Huang, R., Liu, C., and Zhang, T.: Impact of city lockdown on the air quality of COVID-19-hit of Wuhan  
358 city, *Sci. Total Environ.*, 742, 140556, 2020.

359 Luo, Z.: The impact of new outbreak on economy, capital market and national governance and its response, *Finance Economy*,  
360 2020(2), 8–15 ,2020.

361 Ministry of Environmental Protection of China.  
362 [http://www.mee.gov.cn/xxgk2018/xxgk/xxgk05/201903/t20190306\\_694550.html](http://www.mee.gov.cn/xxgk2018/xxgk/xxgk05/201903/t20190306_694550.html), 2019.

363 Niu, F., Li, Z., Li, C., Lee, K., and Wang, M: Increase of wintertime fog in China: Potential impacts of weakening of the  
364 Eastern Asian monsoon circulation and increasing aerosol loading, *J. Geophys. Res.*, 115, D7, 2020.

365 Park, R.: Natural and transboundary pollution influences on sulfate-nitrate-ammonium aerosols in the United States:  
366 Implications for policy, *J. Geophys. Res. Atmos.*, 109, D15204, 2004.

367 Shi, X., and Brasseur, G.: The Response in Air Quality to the Reduction of Chinese Economic Activities during the COVID  
368 Outbreak, *Geophys. Res. Lett.*, 2020, 47, 2020.

369 Shi, Y., Hu, F., LÜ R., and He, Y.: Characteristics of urban boundary layer in heavy haze process based on beijing 325m tower  
370 data, *Atmos. Oceanic Sci. Lett.*, 12, 41–49, 2019.

371 Song, L., Wang, L., Chen, W., and Zhang, Y.: Intraseasonal Variation of the Strength of the East Asian Trough and Its  
372 Climatic Impacts in Boreal Winter, *J. Climate*, 29 (7), 2557–2577, <https://doi.org/10.1175/JCLI-D-14-00834.1>, 2016.

373 Sun, Y., Lei, L., Zhou, W., Chen, C., and Worsnop, D. R.: A chemical cocktail during the COVID-19 outbreak in Beijing,  
374 China: Insights from six-year aerosol particle composition measurements during the Chinese New Year holiday. *Sci. Total  
375 Environ.*, 140739, 2020.

376 Thornton, J. A., Jaegle, L., and McNeill, V. F.: Assessing known pathways for HO<sub>2</sub> loss in aqueous atmospheric aerosols:  
377 Regional and global impacts on tropospheric oxidants, *J. Geophys. Res.-Atmos.*, 113, D05303,  
378 <https://doi.org/10.1029/2007jd009236>, 2008.

379 Tian, H., Liu, Y., Li, Y., Wu, C., Chen, B., Kraemer, M., Li, B., Cai, J., Xu, B., Yang, Q., Wang, B., Yang, P., Cui, Y., Song, Y.,  
380 Zheng, P., Wang, Q., Bjornstad, O., Yang, R., Grenfell, B., Pybus, O., Dye, C.: An investigation of transmission control  
381 measures during the first 50 days of the COVID-19 epidemic in China, *Science*, eabb6105, 2020.

382 Wang, H., and Jin, Y.: The Study on Air Pollution Effects on the Mechanism of Respiratory System. *Science of Travel  
383 Medicine*, 007(002), 29–33, 2001.

384 Wang, P., Chen, K., Zhu, S., Wang, P., and Zhang, H.: Severe air pollution events not avoided by reduced anthropogenic  
385 activities during COVID-19 outbreak, *Resour. Conserv. Recy.*, 158, <http://doi:10.1016/j.resconrec.2020.104814>, 2020.

386 Wang, Y., Li, W., Gao, W., Liu, Z., Tian, S., Shen, R., Ji, D., Wang, S., Wang, L., Tang, G., Tao, S., Cheng, M., Wang, G., Gong,  
387 Z., Hao, J., and Zhang, Y.: Trends in particulate matter and its chemical compositions in China from 2013–2017, *Sci. China  
388 Ser. D.*, 62(12), 1857–1871, 2019.

389 Xia, J., and Feng, X.: Impacts of COVID-19 epidemic on tourism industry and related countermeasures, *Chinese Business and  
390 Market*, 34(3), 3–10, 2020.

391 Xiao, D., Li, Y., Fan, S., Zhang, R., Sun, J., and Wang, Y.: Plausible influence of Atlantic Ocean SST anomalies on winter haze  
392 in China. Plausible influence of Atlantic Ocean SST anomalies on winter haze in China, *Theor. Appl. Climatol.*, 122, 249–257,  
393 2015.

394 Yang, Y., Liao, H., and Lou, S.: Increase in winter haze over eastern China in recent decades: Roles of variations in  
395 meteorological parameters and anthropogenic emissions, *J. Geophys. Res. Atmos.*, 121, 13050–  
396 13065, <https://doi.org/10.1002/2016jd025136>, 2016.

397 Yin, Z., and Wang, H.: The relationship between the subtropical Western Pacific SST and haze over North-Central North China  
398 Plain, *Int. J. Climatol.*, 36, 3479–3491, 2016.

399 Yin, Z., and Wang, H.: Role of atmospheric circulations in haze pollution in December 2016, *Atmos. Chem. Phys.* 17, 11673–  
400 11681. <https://doi.org/10.5194/acp-17-11673-2017>, 2017.

401 Yin, Z., Wang, H., and Guo, W.: Climatic change features of fog and haze in winter over North China and Huang-Huai Area,  
402 *Sci. China Ser. D.*, 58, 1370–1376, 2015.

403 Yin, Z., and Zhang, Y.: Climate anomalies contributed to the rebound of PM<sub>2.5</sub> in winter 2018 under intensified regional air  
404 pollution preventions, *Sci. Total Environ.*, 726, 138514, 2020.

405 Yu, F., and Luo, G.: Simulation of particle size distribution with a global aerosol model: Contribution of nucleation to aerosol  
406 and CCN number concentrations, *Atmos. Chem. Phys.*, 9, 7691-7710, 2009.

407 Zhang, X., Xu, X., Ding, Y., Liu, Y., Zhang, H., Wang, Y., Zhong, J.: The impact of meteorological changes from 2013 to 2017  
408 on PM<sub>2.5</sub> mass reduction in key regions in China, *Sci. China Ser. D.*, 62, 1885–1902, <https://doi.org/10.1007/s11430-019-9343-3>, 2020.

410 Zhou, W., Gao, M., He, Y., Wang, Q., Xie, C., Xu, W., Zhao, J., Du, W., Qiu, Y., Lei, L., Fu, P., Wang, Z., Worsnop, D., Zhang,  
411 Q., and Sun, Y.: Response of aerosol chemistry to clean air action in Beijing, China: Insights from two-year ACSM  
412 measurements and model simulations, *Environ. Pollut.*, 255, 113345, 2019.

413 Zou, Y., Wang, Y., Zhang, Y., and Koo, J.: Arctic sea ice, Eurasia snow, and extreme winter haze in China, *Sci. Adv.*, 3,  
414 e1602751, 2017.

415

416

417

418

419

420

421

422

423

424

425

426

427

428

429

430

431

432

433

**Figure Captions**

435 **Figure 1.** (a) Variation in existing confirmed cases (bar; red: increase, blue: decrease) and the ratio of accumulated confirmed  
 436 cases to total confirmed cases (black line) in China. (b) The ratio of work resumption in large industrial enterprises in the east  
 437 of China. (c) Time of the official 7-days holiday of Chinese New Year from 2013 to 2020.

438 **Figure 2.** (a) Spatial distribution of observed (dots) and GEOS-Chem simulated (shading)  $\text{PM}_{2.5}$  (unit:  $\mu\text{g}/\text{m}^3$ ) in February  
 439 2017. Observed  $\text{PM}_{2.5}$  concentrations (black, unit:  $\mu\text{g}/\text{m}^3$ ) and simulated  $\text{PM}_{2.5}$  concentrations under 2010 emission (red) and  
 440 1985 emission (blue) in February 2020 in (b) North China (NC), (c) Yangtze River Delta (YRD) and (d) Hubei Province (HB).

441 **Figure 3.** Differences in the observed  $\text{PM}_{2.5}$  (unit:  $\mu\text{g}/\text{m}^3$ ) in February between 2020 and 2017. The black boxes indicate the  
 442 locations of North China (NC, 32.5–42°N, 110–120°E), the Yangtze River Delta (YRD, 28–32.5°N, 118–122°E) and Hubei  
 443 Province (HB, 30–32.5°N, 109.5–116°E).

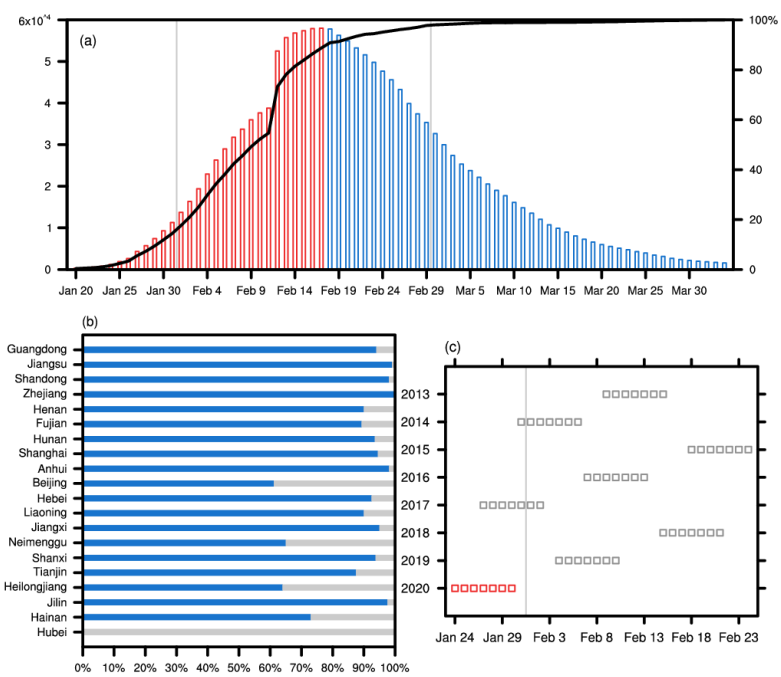
444 **Figure 4.** Differences in the observed atmospheric circulation in February between 2020 and 2017, including (a) geopotential  
 445 potential height at 500 hPa (unit: gpm), (b) wind at 850 hPa (arrows; unit: m/s), surface relative humidity (shading; unit: %).  
 446 The atmospheric circulations in the stagnant days (e.g., from 8–13 and 19–25 February 2020) were also showed, including (c)  
 447 geopotential potential height at 500 hPa (shading; unit: gpm) and its climate mean in February (contour), and (d) wind at 850  
 448 hPa (black arrows; unit: m/s), its climate mean (blue arrows) and the increased surface relative humidity (shading; unit: %,  
 449 stagnant days minus climate mean).

450 **Figure 5.**  $\text{PM}_{2.5}$  difference (unit:  $\mu\text{g}/\text{m}^3$ ) in February between 2020 and 2017 due to (a) changing meteorology ( $\text{PMd}_M$ ), (b)  
 451 expected routine emission reductions ( $\text{PMd}_R$ ), (c) the COVID-19 quarantines ( $\text{PMd}_C$ ), and (d) due to the total emission  
 452 reduction ( $\text{PMd}_E = \text{PMd}_R + \text{PMd}_C$ ).

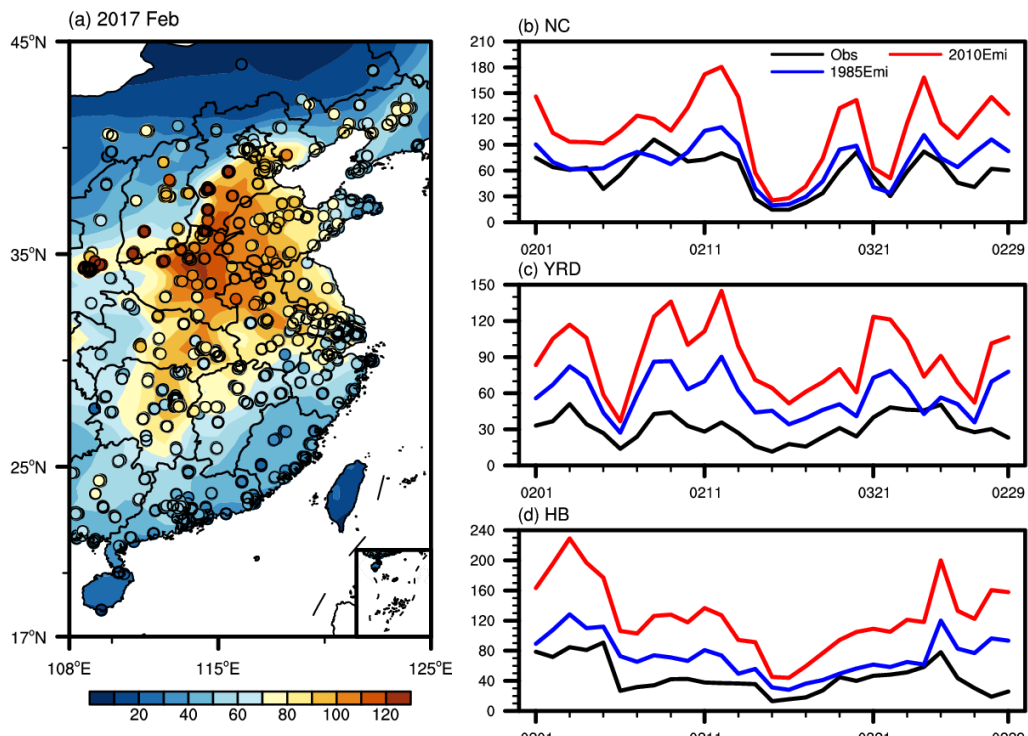
453 **Figure 6.** Variation in  $\text{PMd}_R$  (unit:  $\mu\text{g}/\text{m}^3$ ) with respect to the February 2017 level in Beijing, Shanghai and Wuhan from 2015  
 454 to 2019.  $\text{PMd}_R$  in 2020 was linearly extrapolated from that in the 2015–2019 period. The dotted line is the linear trend.

455 **Figure 7.** Contributions of  $\text{PMd}_M$  (orange bars with hatching),  $\text{PMd}_R$  (purple bars with hatching) and  $\text{PMd}_C$  (blue bars with  
 456 hatching) to the change in  $\text{PM}_{2.5}$  concentration (unit:  $\mu\text{g}/\text{m}^3$ ) between 2020 and 2017 in the three regions. The observed  $\text{PM}_{2.5}$   
 457 concentration in February 2017 (black) and 2020 (gray) was also plotted, and the expected  $\text{PM}_{2.5}$  concentration without the  
 458 COVID-19 quarantine is indicated by black hollow bars. The contribution ratios of the three factors (relative to the  $\text{PM}_{2.5}$   
 459 observations in 2020) are also indicated on the corresponding bars.

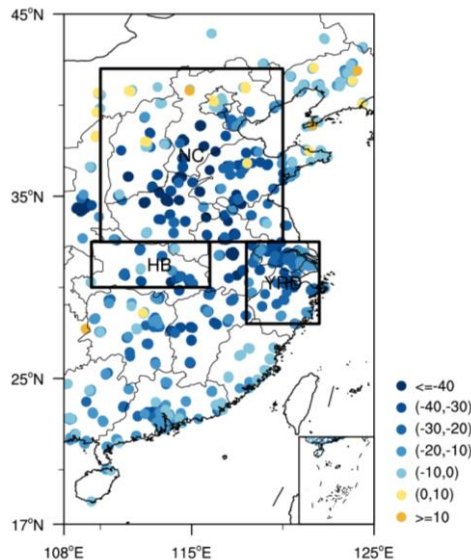
460 **Figure 8.** (a) Differences in the observed  $\text{PM}_{2.5}$  (unit:  $\mu\text{g}/\text{m}^3$ ) in March between 2020 and 2017. (b) Contributions of  $\text{PMd}_C$  to  
 461 the change in  $\text{PM}_{2.5}$  concentration (unit:  $\mu\text{g}/\text{m}^3$ ) between 2020 and 2017 and (c) the contribution ratios of  $\text{PMd}_C$  (relative to the  
 462  $\text{PM}_{2.5}$  observations in 2020) in March (blue) and February (red) in the three regions.



465 **Figure 1.** (a) Variation in existing confirmed cases (bar; red: increase, blue: decrease) and the ratio of accumulated confirmed  
 466 cases to total confirmed cases (black line) in China. (b) The ratio of work resumption in large industrial enterprises in the east  
 467 of China until the end February. (c) Time of the official 7-days holiday of Chinese New Year from 2013 to 2020.

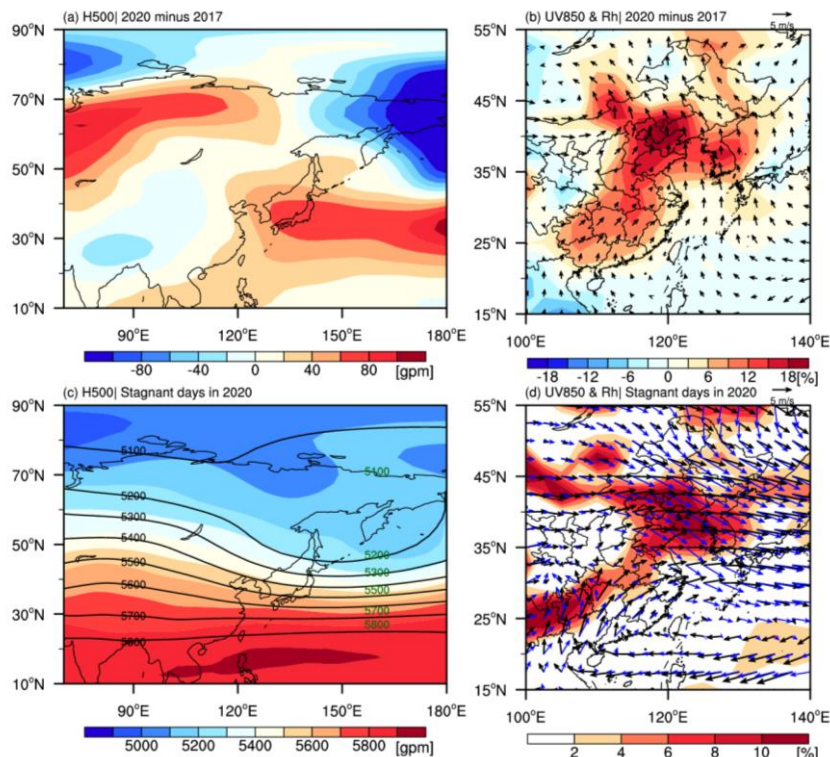


469 **Figure 2.** (a) Spatial distribution of observed (dots) and GEOS-Chem simulated (shading) PM<sub>2.5</sub> (unit:  $\mu\text{g}/\text{m}^3$ ) in February  
 470 2017. Observed PM<sub>2.5</sub> concentrations (black, unit:  $\mu\text{g}/\text{m}^3$ ) and simulated PM<sub>2.5</sub> concentrations under 2010 emission (red) and  
 471 1985 emission (blue) in February 2020 in (b) North China (NC), (c) Yangtze River Delta (YRD) and (d) Hubei Province (HB).



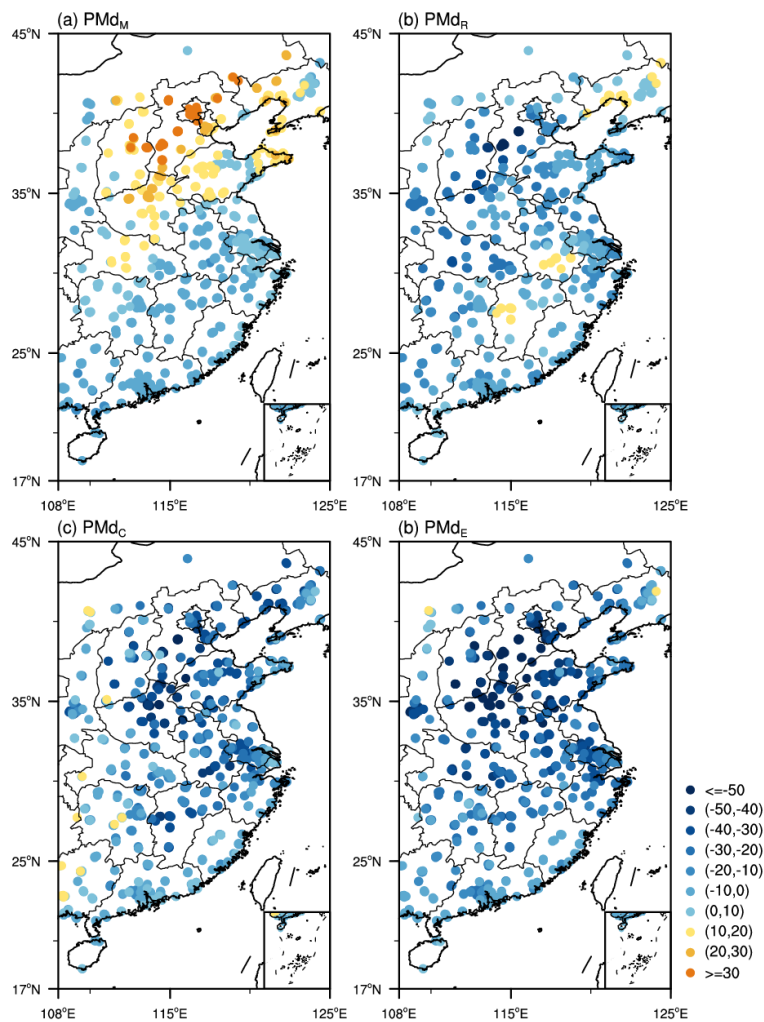
472

473 **Figure 3.** Differences in the observed PM<sub>2.5</sub> (unit:  $\mu\text{g}/\text{m}^3$ ) in February between 2020 and 2017. The black boxes indicate the  
 474 locations of North China (NC, 32.5-42°N, 110-120°E), the Yangtze River Delta (YRD, 28-32.5°N, 118-122°E) and Hubei  
 475 Province (HB, 30-32.5°N, 109.5-116°E).



476

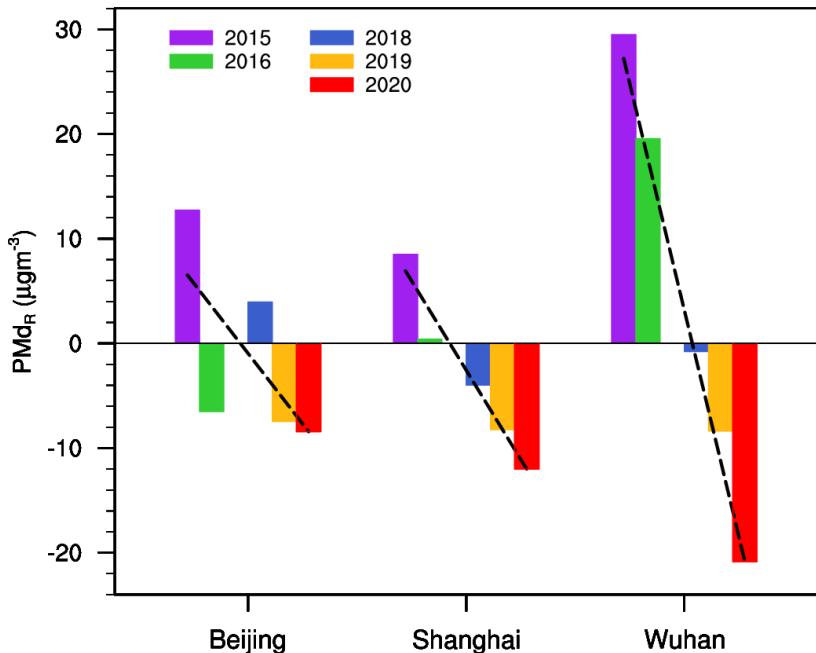
477 **Figure 4.** Differences in the observed atmospheric circulation in February between 2020 and 2017, including (a) geopotential  
 478 potential height at 500 hPa (unit: gpm), (b) wind at 850 hPa (arrows; unit: m/s), surface relative humidity (shading; unit: %).  
 479 The atmospheric circulations in the stagnant days (e.g., from 8–13 and 19–25 February 2020) were also showed, including (c)  
 480 geopotential potential height at 500 hPa (shading; unit: gpm) and its climate mean in February (contour), and (d) wind at 850  
 481 hPa (black arrows; unit: m/s), its climate mean (blue arrows) and the increased surface relative humidity (shading; unit: %,  
 482 stagnant days minus climate mean).



483

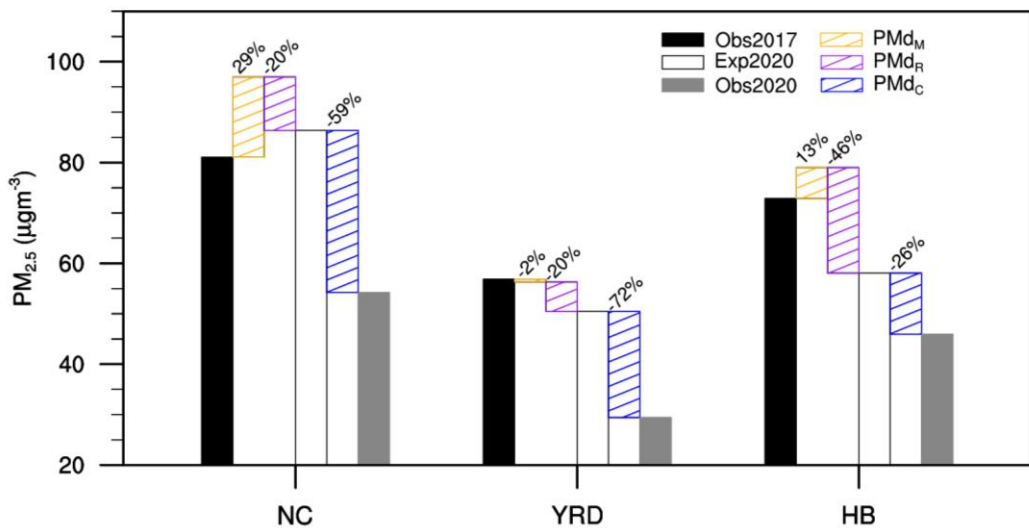
484 **Figure 5.** PM<sub>2.5</sub> difference (unit:  $\mu\text{g}/\text{m}^3$ ) in February between 2020 and 2017 due to (a) changing meteorology (PMd<sub>M</sub>), (b)  
 485 expected routine emission reductions (PMd<sub>R</sub>), (c) the COVID-19 quarantines (PMd<sub>C</sub>), and (d) due to the total emission  
 486 reduction (PMd<sub>E</sub> = PMd<sub>R</sub>+PMd<sub>C</sub>).

487



488

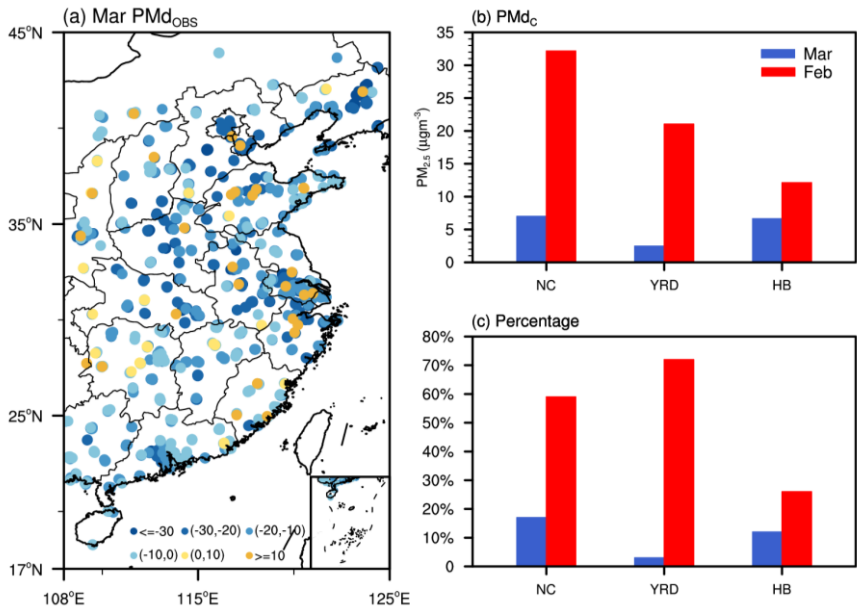
489 **Figure 6.** Variation in  $\text{PMd}_R$  (unit:  $\mu\text{g}/\text{m}^3$ ) with respect to the February 2017 level in Beijing, Shanghai and Wuhan from 2015  
490 to 2019.  $\text{PMd}_R$  in 2020 was linearly extrapolated from that in the 2015–2019 period. The dotted line is the linear trend.



491

492 **Figure 7.** Contributions of  $\text{PMd}_M$  (orange bars with hatching),  $\text{PMd}_R$  (purple bars with hatching) and  $\text{PMd}_C$  (blue bars with  
493 hatching) to the change in  $\text{PM}_{2.5}$  concentration (unit:  $\mu\text{g}/\text{m}^3$ ) between 2020 and 2017 in the three regions. The observed  $\text{PM}_{2.5}$   
494 concentration in February 2017 (black) and 2020 (gray) was also plotted, and the expected  $\text{PM}_{2.5}$  concentration without the  
495 COVID-19 quarantine is indicated by black hollow bars. The contribution ratios of the three factors (relative to the  $\text{PM}_{2.5}$   
496 observations in 2020) are also indicated on the corresponding bars.

497



498

499 **Figure 8.** (a) Differences in the observed  $\text{PM}_{2.5}$  (unit:  $\mu\text{g}/\text{m}^3$ ) in March between 2020 and 2017. (b) Contributions of  $\text{PMd}_C$  to  
500 the change in  $\text{PM}_{2.5}$  concentration (unit:  $\mu\text{g}/\text{m}^3$ ) between 2020 and 2017 and (c) the contribution ratios of  $\text{PMd}_C$  (relative to the  
501  $\text{PM}_{2.5}$  observations in 2020) in March (blue) and February (red) in the three regions.

502

503